J. Fluid Mech. (1971), *vol.* 47, *part* 4, *pp.* 811–824
Printed in Great Britain

Shallow-water waves, the Korteweg–deVries equation and solitons

By N. J. ZABUSKY
Bell Telephone Laboratories, Whippany, N. J. 07981
AND C. J. GALVIN
U.S. Army Coastal Engineering Research Center
Washington, D.C.

(Received 6 October 1970)

A comparison of laboratory experiments in a shallow-water tank driven by an oscillating piston and *numerical* solutions of the Korteweg–deVries (KdV) equation show that the latter can accurately describe slightly dissipative wave-propagation for Ursell numbers ($h_1 L^2/h_0^3$) up to 800. This is an input–output experiment, where the initial condition for the KdV equation is obtained from upstream (station 1) data. At a downstream location, the number of crests and troughs and their phases (or relative locations within a period) agree quantitatively with numerical solutions. The crest-to-trough amplitudes disagree somewhat, as they are more sensitive to dissipative forces. This work firmly establishes the soliton concept as necessary for treating the propagation of shallow-water waves of moderate amplitude in a low-dissipation environment.

1. Introduction

The KdV equation (1895),

$$h_t + hh_x + \delta^2 h_{xxx} = 0, \tag{1.1}$$

was first derived as an asymptotic description of small-but-finite (i.e. laminar) shallow-water waves, where nonlinear and dispersive wave effects compete, and dissipative effects can be neglected. In recent years, the KdV equation has been derived as an essential model equation for a class of nonlinear dispersive or *loss-less* waves, including magnetohydrodynamics (Gardner & Morikawa 1960), the ion-acoustic plasma (Washimi & Taniuti 1966), and the 'anharmonic' or nonlinear lattice (Zabusky 1967). Generally, a large class of nearly hyperbolic mathematical systems reduce to the KdV equation (Su & Gardner 1969; Tappert & Tang 1969), when one formally assumes small-but-finite amplitude waves propagating in only one characteristic direction (the appropriate conditions for this circumstance to occur have been given by Tappert & Tang 1969).

With digital computers capable of solving (1.1) in relevant physical situations, we can now 'close the loop' of reasoning between asymptotic analysis and experimental reality. The classic pattern of smooth long waves transforming into a train or 'wavelets' (sometimes called secondary waves) was discovered computationally by Zabusky, Kruskal & Deem (Zabusky & Kruskal 1965; Zabusky,

Deem & Kruskal 1965) when they solved (1.1) with periodic boundary conditions. These solitary wave-like undulations were designated 'solitons', because they are related to the solitary wave on the infinite line or the cnoidal wave for periodic solutions of (1.1), and because they are stable entities (like particles) that preserve their form through many interactions. Peregrine (1966) solved an equation equivalent to (1.1); and Madsen & Mei (1969) solved a more complete set of equations in one dimension, and also observed two or more solitons form from a single soliton as it propagated into a shallower region (soliton 'fission' on a shelf).

The existence of solitary waves in shallow water has been known for some time. However, the unusual transformations of smooth large amplitude wave-forms in shallow water was first observed by Goda, Takeda & Moriya (1967). Multer & Galvin (1967) observed these transformations and the unusual interactions of primary and secondary waves (solitons). R. Meyer, when viewing the film by Zabusky *et al.* (1965),† observed that the wavelet interactions were similar to those obtained by Galvin (1968) in a sinusoidally driven shallow-water wave tank. An initial experimental/computational study (Zabusky & Galvin 1968) demonstrated that these wavelets are closely related to solutions of the KdV equation, and are some form of soliton. Recently, Madsen, Mei & Savage (1970) re-examined the Galvin (1968) data, and in the first part of their work presented a qualitative and weakly coupled comparison of the experiments with numerical solutions obtained by the complete one-dimensional numerical scheme of Madsen & Mei (1969). The essential behaviour of solitons is not elucidated.

In the last two years the qualitative fissioning into wavelets or solitons and soliton interactions has also been observed in several experiments, including plasma ion-acoustic waves (Ikezi, Taylor & Baker 1970) and electrical transmission lines (Hirota & Suzuki 1970). In another context the KdV equation has been shown to be applicable to thermally excited phonon packets in low temperature, nonlinear crystal experiments (Tappert & Varma 1970).

In this paper we establish *quantitatively* the soliton concept and the validity of the KdV equation. Small-but-finite amplitude sinusoidal shallow-water waves are launched in a tank, such that the Ursell number varies from 22 to 777. This is an input–output comparison and height data are taken at two well-separated stations.

In § 2 and figure 3 we present the dependent variables and normalizations used to describe: exact solutions to the complete partial differential equations; raw data; smoothed and normalized data; and numerical solutions of the KdV equation. These are assembled tersely in appendix B to aid the reader. In § 3 we describe the experimental configuration, and illustrate how the data from station 1 (S 1) are processed to set up the initial condition for the numerical KdV solver.

† Contents as follows. Part 1: numerical solutions of the KdV equation

$$u_t + uu_x + \delta^2 u_{xxx} = 0,$$

with periodic boundary conditions. Part 2: interaction of a compressive and a rarefractive soliton; solutions of the equation $u_t + u^2 u_x + \delta^2 u_{xxx} = 0$, with periodic boundary conditions. Part 3: numerical solutions for an anharmonic lattice initially excited by an intense localized pulse. This 16 mm, silent, black-and-white film runs 35 min. Available on loan from the Film Library, Bell Telephone Laboratories, Murray Hill, N.J. 07971.

In §4 we compare the numerically computed solutions with the data measured at the downstream station (S 2).

The advantages of the KdV level of description are its terseness (one easily compares the dispersive and nonlinear effects) and its computational and analytical tractability. Since the linear wave speed has been transformed out of (1.1), one can take relatively large computational steps. Furthermore, an exact solution of (1.1) has been obtained by Gardner *et al.* (1967) for the infinite line, when an initial state fissions into solitons plus an undular state. The formation and interaction of the pure soliton states are also described by the conservation laws obtained for (1.1) (Zabusky 1967; Miura, Gardner & Kruskal 1968; Kruskal *et al.* 1970).

2. The normalized Korteweg–deVries equation

Starting with equations for a two-dimensional inviscid, incompressible, irrotational fluid in a gravitational field (g), one can derive the first-order dimensional KdV equation

$$(h^*)_{t^*} + (2c_0^*/L^*)\,(h^*)_{x^*} + (3c_0^*/2)\,[(h^* - h_0^*)/h_0^*]\,(h^*)_{x^*} + (c_0^* h_0^{*3}/6h_{11}^*)\,(h^*)_{x^*x^*x^*} = 0 \quad (2.1)$$

for the motion of the *first-order approximation* of the free surface, h^*. The asterisk indicates dimensional *true* values of the variables, and $h^*(x^*, t^*)$ is the exact solution of (2.1). (See appendix B for summary of notation and normalizations.) Equation (2.1) is valid in the limit

$$\epsilon^* \equiv h_{11}^*/h_0^* \ll 1 \quad \text{and} \quad \bar{\epsilon}^* \equiv (h_0^*/L^*)^2 \ll 1, \quad (2.2)$$

where h_0^* is the still-water level, L^* is the fundamental period of the wave,

$$h_{11}^* = \max_{x^*}[h^*(x^*, t_1^*) - h_0^*], \quad (2.3)$$

where h_{11}^* measures the finiteness of amplitude, and where t_1^* is an early time in our experiment (e.g. when the wave passes the upstream or S 1 probe as shown in figure 1 (a)). The linear wave speed is

$$c_0^* = (gh_0^*)^{\frac{1}{2}}, \quad (2.4)$$

and time normalizations are

$$t_0^* = h_0^*/c_0^* = (h_0^*/g)^{\frac{1}{2}} \quad \text{and} \quad T^* = L^*/c_0^*. \quad (2.5)$$

We now assume we are dealing with smoothed measured quantities (subject to small measurement and data smoothing errors) and suppress the asterisk. If we transform to a frame of reference moving with the linear wave-speed, $c_0 = (gh_0)^{\frac{1}{2}}$, then (2.1) becomes

$$\tilde{h}_t + \tilde{h}\tilde{h}_x + \delta_0^2 \tilde{h}_{xxx} = 0, \quad (2.6)$$

where

$$\left.\begin{aligned} &\tilde{h} = \tilde{h}(\tilde{x}, \tilde{t}) = (h - h_0)/h_{11} \quad (\text{note } \max_{\tilde{x}} \tilde{h}(\tilde{x}, \tilde{t}_1) = 1{\cdot}0), \\ &\tilde{t} = 3h_{11}t/Lt_0 = 3h_{11}t/h_0 T, \\ &\tilde{x} = 2(x - c_0 t)/L, \\ &\delta_0^2 = 4/9Ur_0 = 4h_0^3/9h_{11}L^2 = 4h_0^2/9gh_{11}T^2, \\ &\text{and} \quad Ur_0 = \epsilon/\bar{\epsilon} = h_{11}L^2/h_0^3 \end{aligned}\right\} \quad (2.7a\text{–}e)$$

is the Ursell number, analogous to the Reynolds number for nonlinear dissipative systems. Note that there is an ambiguity in defining Ur_0 or δ_0^2, for as (2.3) shows, h_{11} is dependent on t_1, and if the wave-form is evolving, h_{11} will change.

Below we describe the manner in which the experiment was conducted and justify the use of periodic boundary conditions, namely

$$h^*(x^*) = h^*(x^* + L^*) \quad \text{or} \quad \tilde{h}(\tilde{x}) = \tilde{h}(\tilde{x} + 2). \tag{2.8}$$

That is, *time elapsed in the numerical computation is related to the distance between* S 1 *and a downstream location of the propagating wave.*

3. Experimental configuration

Experiments were performed in a tank 96 ft long and 1·5 ft wide. Waves were launched on water at two heights (0·242 ft and 0·493 ft) by an oscillating piston upstream and dissipated on a beach, as shown in figure 1 (*a*). The disturbance of the free surface height from the still-water level was measured by fixed resistive probes mounted vertically. An upstream probe (S 1) close to the oscillator recorded a nearly sinusoidal signal that was digitized to give $\hat{h}_1(\hat{x})$, where $\hat{x}$ is taken at discrete temporal intervals. A downstream probe (S 2) also measured an undular signal and was digitized to give $\hat{h}_2(\hat{x})$, where $\hat{x}$ is a discretized temporal variable. Figure 1 (*b*) shows a typical S 2 wave-form. Tables 1 and 2 give the parameters of the three experiments and the results of five numerical computations. In referring to entries in tables we will use the notation $A:X$ for table A, row X and $A:X, Y$ for table A, row X, column Y. The columns are, of course, the labels for the cases considered.

Now we justify the use of periodic boundary conditions (2.8) to describe the evolution of waves propagating past two separated stations. Figure 2 shows a Clevite–Brush recording of the wave-form at S 2. As the wave passes the probe, it produces a temporal signal that is translated into spatial form by the recorder. After about two periods, the wave-form remains nearly constant (less than 1 % variation at tallest crests from period-to-period) until the arrival of the weak signals reflected from the beach. The data at S 2, compared with the numerical solutions (as described below), are usually taken from period 2 or higher of a given recording. The number of raw data points in a period is shown in entries 1:9 and 1:10, (N_{p1}) for S 1 and (N_{p2}) for S 2. For two of the three runs the periodicity assumption holds 0·025 %. Hence, if the two probes are separated by a 'proper' distance S_{12} then time elapsed in the numerical computation t_{12} is

$$t_{12} \simeq S_{12}/c_0. \tag{3.1}$$

The 'proper' distance is chosen to be sufficiently large to observe the initial smooth wave-form develop its full complement of undulations (solitons-to-be), but also small enough that the leading 'zero-crossing' (see figure 1 (*b*)) does not propagate to the right into the preceding period. Entry 1:5 shows distances of about 20 ft or $2{\cdot}23 < (S_{12}/L) < 2{\cdot}43$. The data will also be validated by examining how well (3·1) is satisfied.

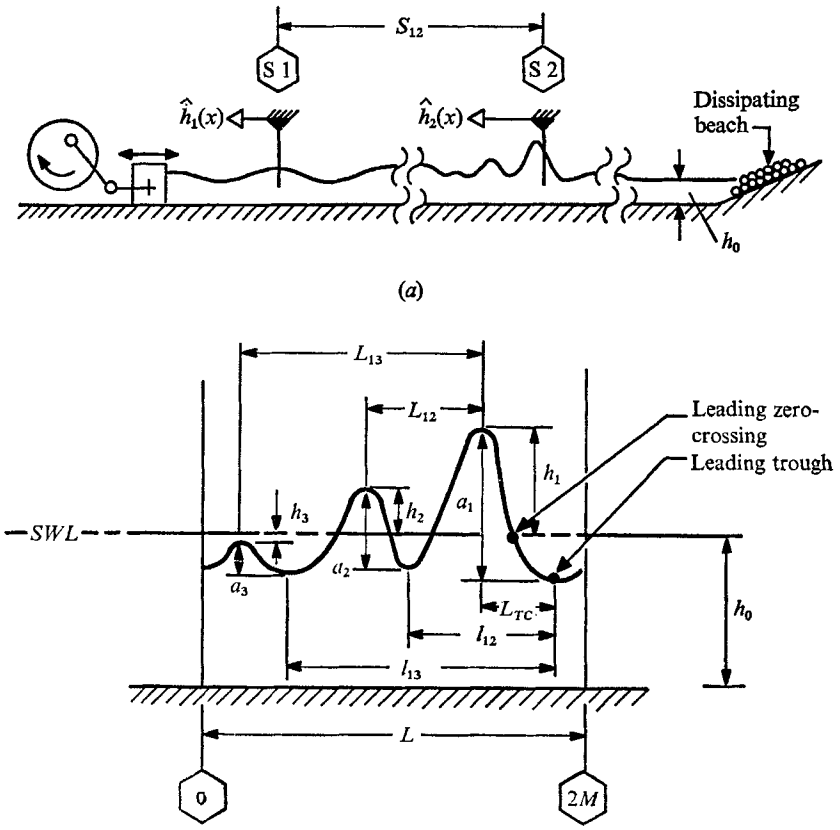

FIGURE 1. (*a*) A schematic diagram illustrating a shallow-water wave tank driven by an oscillating piston and data recorded at two properly separated stations. (*b*) Typical undular wave-form recorded at S 2.

3.1. *Smoothing, computing and validating procedures*

Figure 3 illustrates how the data are smoothed and coupled to the KdV numerical algorithm for initialization and comparisons. Properties of the KdV algorithm have been given previously (Zabusky 1968) and are summarized briefly in appendix A. In what follows we assume that unnormalized raw and smoothed data are dimensional.

(i) The raw data, $\hat{h}_1(\hat{x})$ at S 1 and $\hat{h}_2(\hat{x})$ at S 2, are fitted with trigonometric functions using a conventional least-squares procedure. The Fourier cosine and sine amplitudes, A_{ik} and B_{ik}, ($k \geqslant 1$), of N_{H1} harmonics ($i = 1$ for S 1) and N_{H2} ($i = 2$ for S 2) harmonics, are computed to adequately represent the data. Entries 1:9 and 1:10 show that between 6 and 8 harmonics were used to represent S 1 data, and between 14 and 20 harmonics were used to represent S 2 data.

(ii) The unnormalized zero-mean input and test functions $h_1(x_m)$ and $h_2(x_m)$ are computed at $2M$ points $1 \leqslant x_m \leqslant 2M$ in a period using N_{Hi} amplitudes obtained in the previous step. Entry 1:19 gives the value of $2M$. We usually took

$M < N_{pi}/5$, depending upon the resolution required. Entries 1:11 and 1:12 give the normalized mean-square content of a period, where

$$E_i = (2M)^{-1} \sum_{m=1}^{2M} h_i^2(x_m) = \frac{1}{2} \sum_{k=1}^{N_{Hi}} (A_{ik}^2 + B_{ik}^2), \tag{3.2}$$

and

$$h_{11} = \max_{x_m} h_1(x_m) - h_0. \tag{3.3}$$

E_{1x}/h_{11}^2 and E_{2x}/h_{11}^2, given in entries 1:13 and 1:14, are the normalized square content of the highest harmonic used and give one an estimate of the error made in omitting the last harmonic. For example, in column 5, where $N_{H1} = 6$, the fraction of energy in the sixth harmonic is $2{\cdot}2 \times 10^{-4}$ of the total energy, E_1.

	Case	1	2	3	4	5
(1)	h_0(ft)	0·493	0·242	0·242	0·493	0·242
(2)	L(ft)	7·92	8·38	9·46	7·92	8·38
(3)	c_0(ft/sec)	3·98	2·79	2·79	3·98	2·79
(4)	T (sec)	1·99	3·00	3·39	1·99	3·00
(5)	S_{12}(ft)	19·2	18·7	21·2	19·2	18·7
(6)	h_{11}(ft)	0·0418	0·0192	0·0243	0·0418	0·0192
(7)	S_{12}/L	2·43	2·23	2·24	2·43	2·23
(8)	h_{11}/h_0	0·0848	0·0793	0·1004	0·0848	0·0793
(9)	N_{P1}/N_{H1}	392/8	584/6	663/8	392/7	584/6
(10)	N_{P2}/N_{H2}	392/15	582/16	664/20	392/14	582/15
(11)	E_1/h_{11}^2	0·4423	0·4679	0·4334	0·4423	0·4679
(12)	E_2/h_{11}^2	0·3784	0·4087	0·3908	0·3784	0·4087
(13)	E_{1x}/h_{11}^2	$0{\cdot}83 \times 10^{-6}$	$0{\cdot}51 \times 10^{-4}$	$0{\cdot}47 \times 10^{-4}$	$0{\cdot}45 \times 10^{-5}$	$0{\cdot}10 \times 10^{-3}$
(14)	E_{2x}/h_{11}^2	$0{\cdot}29 \times 10^{-6}$	$0{\cdot}68 \times 10^{-6}$	$0{\cdot}50 \times 10^{-6}$	$0{\cdot}41 \times 10^{-6}$	$0{\cdot}13 \times 10^{-4}$
(15)	$(\Delta E)_p$	5·9	5·6	4·4	5·9	5·6
(16)	Ur_0	21·95	481·6	777·0	21·95	481·6
(17)	δ_0^2	0·02025	0·004672	0·002896	0·02025	0·004672
(18)	δ^2	0·02025	0·004672	0·002896	0·0229	0·004043
(19)	$2M$	140	200	260	100	220
(20)	Δt (msec)	0·282	0·671	0·443	0·772	0·505
(21)	N_{c0}	17,125	9,943	17,165	6,240	13,235
(22)	N_c	19,978	10,069	15,814	7,009	12,232

TABLE 1. Parameters describing experiment and computation

Note that in all cases $E_2/h_{11}^2 < E_1/h_{11}^2$, indicating that energy has been lost. The normalized energy lost per period,

$$(\Delta E)_p = (100\ \%)\,(1 - E_2/E_1)/(S_{12}/L), \tag{3.4}$$

is given in entry 1:15. This observed energy loss of between 10 % and 15 % in less than $2\frac{1}{2}$ periods is not described by the KdV equation and accounts mostly for the small amplitude discrepancies we observe in comparing measured and computed results in §4.

(iii) The data are now normalized:

$$\tilde{h}_1(x_m) = h_1(x_m)/h_{11}, \tag{3.5}$$

$$\tilde{h}_2(x_m) = h_2(x_m)/h_{11}; \tag{3.6}$$

	Case	1		2		3		4		5	
(1)	Ur_0	21·95		481·6		777·0		21·95		481·6	
(2)	δ_0^2	0·02025		0·004672		0·002896		0·02025		0·004672	
(3)	δ^2	0·02025		0·004672		0·002896		0·0229		0·004043	
(4)	$\epsilon(t_c)/h_{11}^2$	0·0035		0·0040		0·0068		0·006		0·0095	
(5)	S_c/L	2·83		2·26		2·06		2·73		2·06	
(6)	$(S_{12}-S_c)/S_{12}$	0·166		0·0134		−0·0788		0·123		−0·076	
	(S 2)	Data	KdV	Data	KdV	Data	KdV	Data	KdV	Data	KdV
(7)	h_1/h_{11}	1·40	1·51	1·75	1·96	1·89	2·10	1·40	1·44	1·75	2·04
(8)	h_2/h_{11}	−0·31	−0·35	0·69	0·64	0·79	0·87	−0·31	−0·42	0·69	0·73
(9)	h_3/h_{11}	—	—	−0·11	−0·14	0·067	0·097	—	—	−0·1	−0·053
(10)	a_1/h_{11}	1·83	2·21	2·46	2·74	2·60	2·84	1·83	1·99	2·46	2·83
(11)	a_2/h_{11}	0·23	0·10	0·78	0·71	0·90	1·12	0·23	0·11	0·78	0·88
(12)	a_3/h_{11}	—	—	0·10	0·004	0·24	0·17	—	—	0·10	0·062
(13)	L_{TC}/L	0·30	0·30	0·20	0·19	0·17	0·17	0·31	0·32	0·20	0·18
(14)	L_{12}/L	0·50	0·55	0·23	0·23	0·21	0·21	0·50	0·51	0·24	0·23
(15)	L_{13}/L	—	—	0·45	0·44	0·43	0·40	—	—	0·45	0·44
(16)	l_{12}/L	0·47	0·39	0·33	0·31	0·27	0·27	0·40	0·36	0·33	0·30
(17)	l_{13}	—	—	0·58	0·60	0·49	0·49	—	—	0·57	0·55
(18)	1/2M	0·0071	0·0071	0·005	0·005	0·0038	0·0038	0·01	0·01	0·0045	0·0045

TABLE 2. Parameters describing experiment and computation

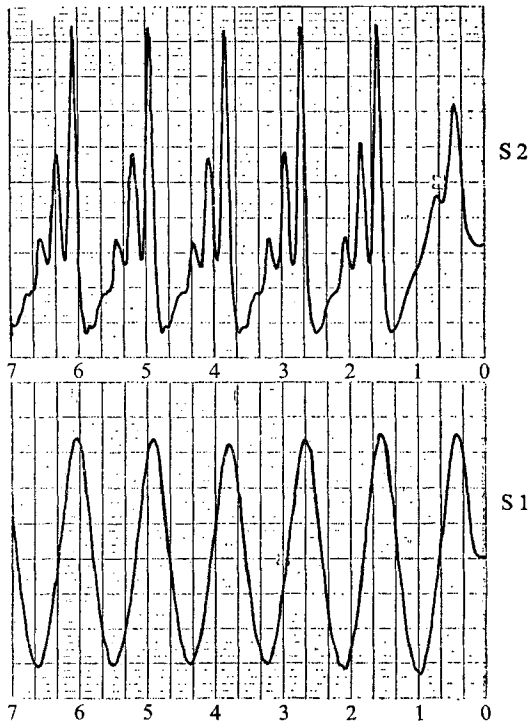

FIGURE 2. Analog recording of S 1 and S 2 wave-forms for case 3, table 1, where $Ur_0 = 777$.

and (3.5) is used as the initial condition for the KdV algorithm. The dispersion parameter for the runs is taken as either

$$\delta_0^2 = 4h_0^3/9h_{11}L^2 \tag{3.7}$$

or some value δ^2 (entry 1:18 or 2:3) near δ_0^2.

(iv) As time evolves a function $\tilde{h}_K(x_m)$ is computed. The normalized S 2 function $\tilde{h}_2(x_m)$ is displaced *discretely*, until its maximum coexists with the maximum of $\tilde{h}_K(x_m, t)$, and an error function is computed

$$\epsilon(t_n) = (2M)^{-1} \sum_{m=1}^{2M} [\tilde{h}_K(x_m, t_n) - \tilde{h}_2(x_m - x_s)]^2, \tag{3.8}$$

where x_s is determined such that (3.9) has a minimum

$$|\max_{x_m} \tilde{h}_K(x_m, t) - \max_{x_m} \tilde{h}_2(x_m - x_s)|. \tag{3.9}$$

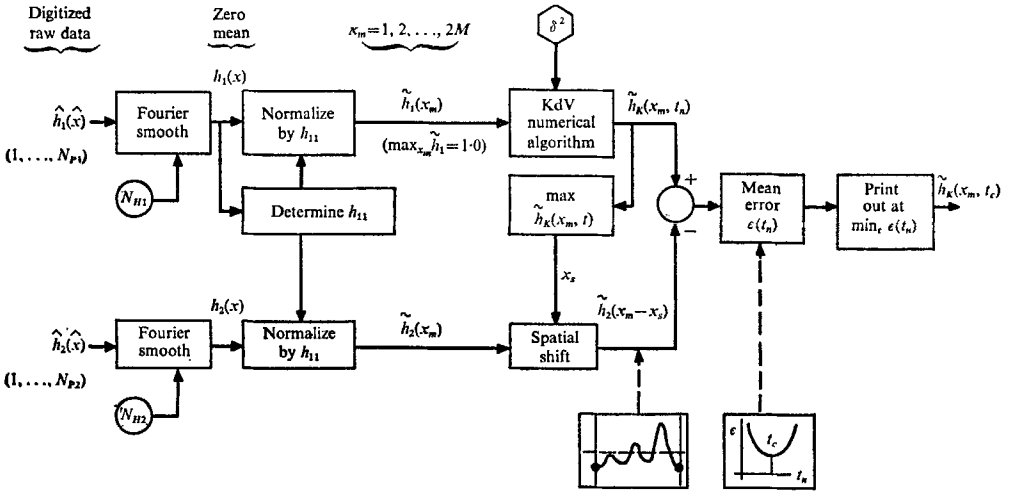

FIGURE 3. Flow chart for smoothing, numerical computing, and validating procedures.

Because of this discreteness, $\epsilon(t_n)$ will be discontinuous in time. The magnitude of the discontinuity is made smaller with M larger.

The wave-form is printed out, together with the value of $\epsilon(t_n)/h_{11}^2$. The time t_c is designated, where ϵ has a minimum (entry 2:4). We define

$$S_c = c_0 t_c, \tag{3.10}$$

and S_c/L is compared to S_{12}/L in entry 2:6.

The number of computation steps to t_c is $N_c = t_c/(\Delta t)$, where

$$\Delta t = \tfrac{9}{48} T(L^2/M^3 h_0^2). \tag{3.11}$$

4. Comparisons: Experiment and computation

The data in tables 1 and 2 are for three different experimental Ursell numbers, entry 1:16 or 2:1. Cases 1, 2 and 3 take $\delta^2 = \delta_0^2$. Cases 4 and 5 have the same data

as cases 1 and 2, respectively, but $\delta^2 \neq \delta_0^2$. We discuss below the effect of errors in measurement of h_{11}, h_0 and L and therefore in the calculation of δ^2.

Remember figure 3 (the flow of information) and figure 1 (*b*) (the definitions of the wave-form parameters)! These are the essence of the comparisons, shown in the lower part of table 2. Our comparisons are made in two almost independent ways. We set up an *a priori* criterion that the computed wave-form $\tilde{h}_K(x_m, t_n)$ correspond to the measured wave-form $\tilde{h}_2(x_m - x_s)$ at that time t_c when the mean-square difference between $\tilde{h}_K$ and $\tilde{h}_2$ is a minimum. Obviously, t_c will vary slightly, if we vary parameters like N_{H1} or N_{H2}, if we include a different criterion (say, minimize the absolute-value difference), or if we include a loss term on the right

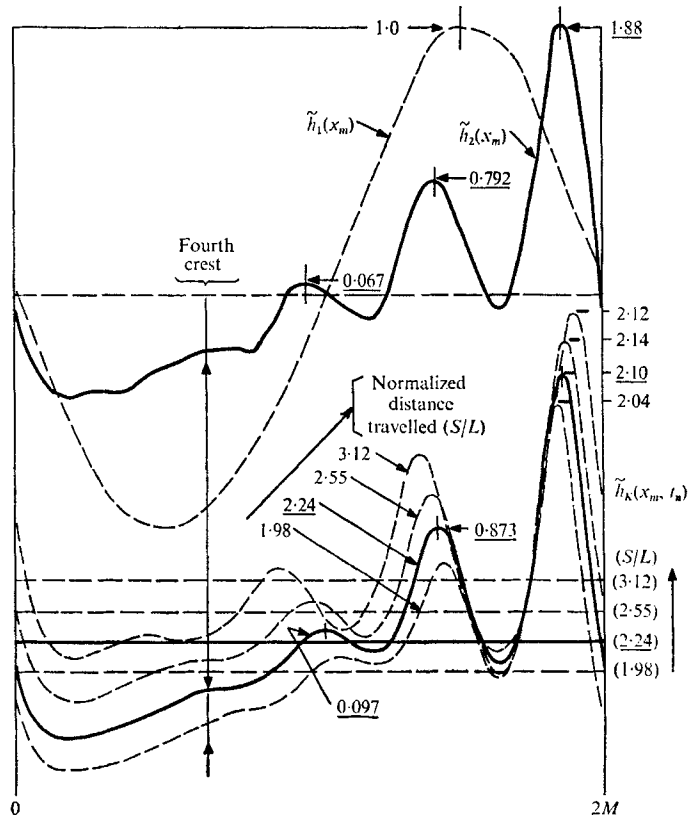

FIGURE 4. Case 3 wave-forms: above $\tilde{h}_1(x_m)$ and $\tilde{h}_2(x_m)$; below $\tilde{h}_K(x_m, t_n)$, where $t_n \propto S/L$ = 1·98, 2·24, 2·55, 3·12. The zero level of each curve is indicated at right. Caution: all graphs are plotted by the computer are normalized to unity. The actual amplitude scales are given at right.

side of (2.6). We next compare the wave-form $\tilde{h}_K(x_m, t_c)$ with $\tilde{h}_2(x_m)$ by examining the normalized *amplitudes*: crests above *SWL* (h_i/h_{11}) and crest-to-trough distances (a_i/h_{11}); and phases (or relative location of crests and troughs) in a period with respect to the leading crest. Normalized amplitudes are given in entries 2:7–2:12 and normalized phase information in entries 2:13–2:17. Figure 1 (*b*) illustrates these normalized quantities. We discuss this information below.

Figure 4 shows six wave-forms relevant to case 3. At the top, $\tilde{h}_1(x_m)$ and $\tilde{h}_2(x_m)$ are plotted, each normalized to unity (retraces of computer output), and actual amplitudes are given at right. Below, four values of $\tilde{h}_K(x_m, t_n)$ are given at normalized distances from S 1 of 1·98, 2·24, 2·55 and 3·12. The solid curve, $S_c/L = 2{\cdot}24$, corresponds to t_c and compares adequately in amplitude and very favourably in phase with $\tilde{h}_2(x_m)$ above. Note that the four lower graphs are each normalized to unity with their zero lines displaced upward. The actual leading crest amplitudes are given at right and the two smaller crests of the solid curve are also labelled. Note that the normalized amplitude of the leading soliton has a maximum value of 2·14 at $S/L = 2{\cdot}55$ and then decreases. This results because the leading soliton is moving into the period ahead and interacting with the fourth crest. We see the well-known effect of the taller soliton decreasing in amplitude, and the smaller growing in amplitude, during a two soliton interaction (Multer & Galvin 1967).

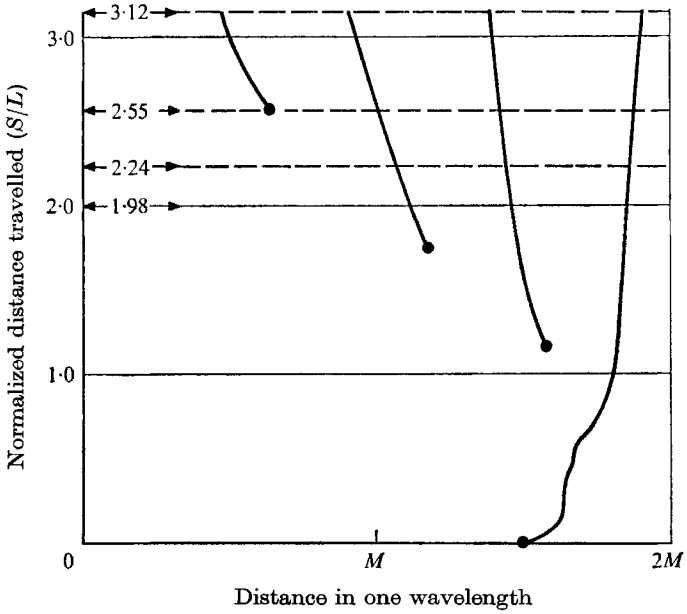

FIGURE 5. Trajectory of crests in a wave period. Case 3, $Ur_0 = 777$.

Figure 5 shows the computed trajectory of crests in a wave period. Conceptually, the observer is translating along with the linear speed c_0. At $S/L = 2{\cdot}55$ a fourth crest develops. Its appearance is expected because of the inflexion point evident in the data in figure 4.

Since the KdV numerical algorithm conserves the mean-square of the wave-form, that is

$$\sum_{m=1}^{2M} \tilde{h}_i^2(x_m, t_n),$$

or the 'energy', and the data do not, one expects and finds that the data amplitudes are smaller than the KdV amplitudes, entries 2:10–2:12. The phases, entries 2:13–2:18, have consistently smaller deviations.

As the Ursell number was increased, the normalized energy decay per period decreased from 5·91 to 4·41 (entries 1:15, 1 and 1:15, 3); the error in the computed separation distance (entry 1:6) decreased, although not consistently; and the phase data (entries 2:13–2:18) showed an improvement as δ_0^2 increased. Also, the mean-square error, $\epsilon(t_c)/h_{11}^2$ (entry 2:4), was always less than 0·7 % in cases 1, 2 and 3, far better than the energy comparison.

The trend of $\epsilon(t_c)/h_{11}^2$ in comparison with $(S_{12}-S_c)/S_{12}$ (entry 2:6) shows $\epsilon(t_c)$ increasing and $(S_{12}-S_c)/S_{12}$ decreasing with increasing Ursell number. The good agreement in $\epsilon(t_c)/h_{11}$ at low Ur follows, because amplitudes are smaller (and the

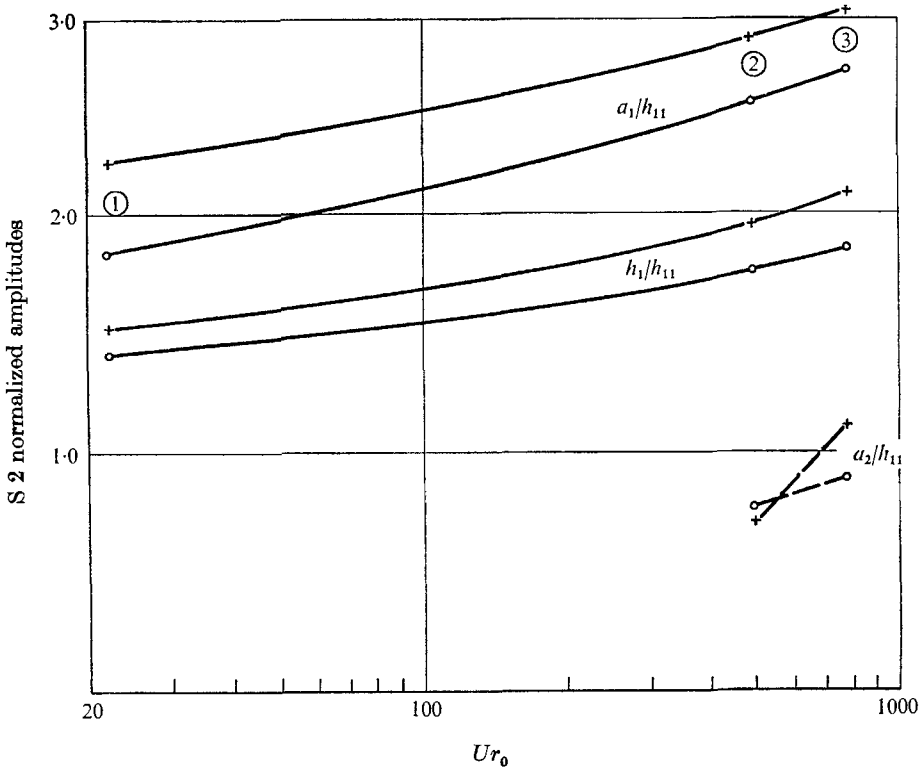

FIGURE 6. Normalized amplitude h_1/h_{11} and a_1/h_{11} and a_2/h_{11} at S 2. A comparison of KdV solutions $\max_{x_m} \tilde{h}_K(x_m, t_n)$ with data $\max_{x_m} \tilde{h}_2(x_m, t)$. ①, ②, ③ refer to cases 1, 2, 3 in tables 1 and 2. +—+, KdV; ○—○, data.

wave-shape is not as undular). However, because of the lack of undular structure at low Ur the $\epsilon(t_n)$ curve has a broader minimum, thus increasing the possibility of error in S_c. To quantify the statements one would have to make a more careful parametric study including dissipation.

The phase information for case 3 is remarkably good, considering the above comments. Only the phase of the smallest crest, L_{13}/L, had an error of 8·25 %. This is to be compared with the error associated with one lattice interval $(1/2M)$ or 0·38 %.

Figure 6 summarizes some of the amplitude results contained in the tables for cases 1, 2 and 3. We see the decrease in amplitude discrepancy between KdV

solutions and smoothed data as the Ursell number increases. The crossing of the a_2/h_{11} curves indicates that we probably must include dissipation in our numerical model if we are to quantify these details.

Case 4 shows that increasing δ^2 by 13 % (compare case 1) decreases the error in S_c (entry 2:6) and greatly improves the amplitude and phase comparisons. It is possible to make a 15 % error in δ^2 because of the h_0^2 in the numerator of (2.7d).

Case 5 shows that decreasing δ^2 by 14% (compare case 2) leads to a degradation in quality in S_c, $\epsilon(t_c)$, amplitude and phase.

5. Conclusions

The Korteweg–deVries equation and the soliton concept can describe the slightly dissipative propagation-and-evolution of finite-amplitude shallow-water waves for Ursell numbers up to 800. As the dissipation becomes weaker, the detail in the comparison of data with KdV numerical solutions becomes better and holds for longer propagation distances. A laboratory-data/numerical-solution comparison of the number of crests and troughs and their phases (or relative locations within a period) shows only negligible difference. As one expects, the crest-to-trough amplitudes differ somewhat more because they are more sensitive to dissipative forces. To quantify some of the details we recommend a study including dissipation.

In some qualitative laboratory experiments we increased the Ursell number above 800, and observed the leading crest grow until its maximum sharpened into a near cusp, i.e. evolved into a maximum-amplitude soliton (analogous to the maximum-amplitude solitary wave). Upon increasing the Ursell number, the leading crest broke by radiating forward a burst of capillary waves. After the capillary waves subsided we were left with a stable propagating crest or soliton followed by its usual train of solitons of decreasing amplitude.

The soliton concept validated here is essential for a terse description of a class of wave-breaking phenomena.

We are grateful for numerous helpful conversations with G. S. Deem and F. Tappert (who also commented on the manuscript) and the programming assistance of J. W. Robinson and Mrs Carol Bateman Tretkoff.

Appendix A. Korteweg–deVries numerical integration algorithm

To advance $\tilde{h}_K(i,j)$ we used a right-to-left sweeping *iterative* algorithm, as validated by Zabusky (1968). The algorithm employed four adjacent points $(i+2,\, i+1,\, i,\, i-1)$ on two time-levels $(j+1, j)$,

$$\tilde{h}_K(i,j+1) = \tilde{h}_K(i+1,j) - [\tilde{h}_K(i+2,j+1) - \tilde{h}_K(i-1,j)]/[(\delta^2+\tilde{F})/(3\delta^2-\tilde{F})], \quad \text{(A 1)}$$

where
$$\tilde{F} = (h^2/8)\,[\tilde{h}_K(i+2,j+1) + \tilde{h}_K(i-1,j)], \quad \text{(A 2)}$$

$h = 1/2M$ is the lattice spacing and the time step is

$$k = h^3/4\delta^2. \quad \text{(A 3)}$$

At a particular time we begin to compute $\tilde{h}_K(2M, j+1)$ using $\tilde{h}_K(2M+1, j)$, $\tilde{h}_K(2M-1, j)$ and a tentative extrapolated value of $\tilde{h}_K^0(2M+2, j+1)$. This extrapolated value is the reason for the iteration. We sweep to the left until we compute $\tilde{h}_K(2, j+1)$ and because of *periodicity* we also designate this

$$\tilde{h}_K^{(1)}(2M+2, j+1).$$

We repeat this process until two successive sweeps differ by a small number, i.e.

$$|1-(\tilde{h}_K^{(n+1)}(2M+2, j+1))/\tilde{h}_K^{(n)}(2M+2, j+1)| < \epsilon', \tag{A 4}$$

where we took $\epsilon' = 10^{-5}$ for the GE-635 computer whose single precision arithmetic carries eight significant figures. The algorithm is second order in h as seen by taking the continuous limit of (A 1).

Appendix B. Summary of variables

We summarize briefly the variables used in this paper.

(i) The starred (*) variables represent 'exact' (hypothetical) dimensional variables; for example, h_0^* is the exact still-water level. However, $h^*(x^*, t^*)$ is the dimensional, first-order asymptotic approximation to the true free surface height and is here assumed to be the exact solution of (2.1) with appropriate boundary conditions. Measured and smoothed *dimensional* quantities are unadorned, e.g. h_0, L, h_{11}, etc.

(ii) Figure 3 shows how the remaining variables are defined:

$\hat{h}_i(\hat{x})$ are the dimensional, digitized, free surface data given at N_{p1} equispaced values of $\hat{x}$ for S 1 ($i = 1$) and N_{p2} equispaced values of $\hat{x}$ for S 2 ($i = 2$).

$h_i(x)$ are the zero-mean, dimensional, smoothed data obtained by selecting the lowest N_{Hi} harmonics for the data at S i and recomposing the function.

$\tilde{h}_i(x_m)$ are the zero-mean, normalized data given at $2M$ equispaced intervals ($1 < x_m < 2M$), corresponding to fundamental period of 2·0.

$\tilde{h}_K(x_m, t_n)$ are the numerical solutions of the KdV equation, with

$$\tilde{h}_K(x_m, 0) = \tilde{h}_1(x_m)$$

as an initial condition and periodic boundary conditions

$$\tilde{h}_K(x_m+2, t_n) = \tilde{h}_K(x_m, t_n).$$

(iii) Note that in figure 1(*b*) the dimensional height of the crest above the still-water level is given as h_1, h_2, h_3, etc. This is an abbreviated notation. If we are discussing smoothed data, the first crest is

$$h_{11} \quad \text{at} \quad \text{S 1}, \quad h_{21} \quad \text{at} \quad \text{S 2, etc.}$$

If we are comparing solutions to the equation with smoothed data then a more complete notation would have

$$h_0\tilde{h}_{K1}(t_c) \quad \text{compared with} \quad h_{21}, \quad h_0\tilde{h}_{K2}(t_c) \quad \text{compared with} \quad h_{22}, \text{ etc.}$$

REFERENCES

GALVIN, C. J. 1968 Finite amplitude, shallow-water waves of periodically recurring form. *U.S. Army Coastal Engineering Research Center.*

GARDNER, C. S., GREENE, J. M., KRUSKAL, M. D. & MUIRA, R. M. 1967 Method for solving the Korteweg–deVries equation. *Phys. Rev. Lett.* **19**, 1095.

GARDNER, C. S. & MORIKAWA, G. K. 1969 Similarity in the asymptotic behaviour of collision-free hydromagnetic waves and water waves. *Courant Institute of Mathematical Science Report* NYO 9082.

GODA, Y., TAKEDA, H. & MORIYA, Y. 1967 Laboratory investigation on wave transmission over breakwaters. *Port and Harbour Research Institute, Yokusaka, Japan, Report* 13.

HIROTA, R. & SUZUKI, K. 1970 Studies on lattice solitons by using electrical networks. *J. Phys. Soc. Japan*, **28**, 1366.

IKEZI, H., TAYLOR, R. J. & BAKER, D. R. 1970 Formation and interaction of ion-acoustic solitary waves. *Phys. Rev. Lett.* **25**, 11.

KORTEWEG, D. J. & DEVRIES, G. 1895 On the change of form on a new type of long stationary waves. *Phil. Mag.* **39**, 422.

KRUSKAL, M. D., MIURA, R. M., GARDNER, C. S. & ZABUSKY, N. J. 1970 Korteweg–deVries equation and generalizations 5. Uniqueness and non-existence of polynomial conservations laws. *J. Math. Phys.* **11**, 1952.

MADSEN, O. S. & MEI, C. C. 1969 The transformation of a solitary wave over an uneven bottom. *J. Fluid Mech.* **39**, 781.

MADSEN, O. S., MEI, C. C. & SAVAGE, R. P. 1970 The evolution of time-periodic long waves of finite amplitude. *J. Fluid Mech.* **44**, 195.

MIURA, R. M., GARDNER, C. S. & KRUSKAL, M. D. 1968 Korteweg–deVries equation and generalizations. 2. Existence of conservation laws and constants of motion. *J. Math. Phys.* **9**, 1204.

MULTER, R. H. & GALVIN, C. J. 1967 Secondary waves: Periodic waves of non-permanent form. (Abstract.) *Trans. Am. Geophys. Union*, **48**, 139.

PEREGRINE, D. H 1966 Calculations of the development of an undular bore. *J. Fluid Mech.* **25**, 321.

SU, C. S. & GARDNER, C. S. 1969 The Korteweg–deVries equation and generalizations. 3. Derivation of the Korteweg–deVries equation and Burgers' equation. *J. Math. Phys.* **10**, 536.

TAPPERT, F. & TANG, J. Y. T. 1969 Nonlinear interaction of finite amplitude waves, 1, 2. *Bell Telephone Laboratories Internal Memorandum.*

TAPPERT, F. & VARMA, C. 1970 Asymptotic theory of self-trapping of heat pulses in solids. *Phys. Rev. Lett.* **25**, 1108.

WASHIMI, H. & TANIUTI, T. 1966 Propagation of ion-acoustic solitary waves of small amplitude. *Phys. Rev. Lett.* **17**, 996.

ZABUSKY, N. J. 1967 A synergetic approach to problems of nonlinear dispersive wave propagation and interaction. *Nonlinear Partial Differential Equations* (ed. W. Ames). New York: Academic Press.

ZABUSKY, N. J. 1968 Solitons and bound states of the time-independent Schrödinger equation. *Phys. Rev.* **168**, 124.

ZABUSKY, N. J., DEEM, G. S. & KRUSKAL, M. D. 1965 Formation, propagation and interaction of solitons (numerical solutions of differential equations describing wave motion in nonlinear dispersive media). (Film.) *Bell Telephone Laboratories, Murray Hill, N.J.*

ZABUSKY, N. J. & GALVIN, C. J. 1968 Secondary waves as solitons. (Abstract.) *Trans. Am. Geophys. Union*, **49**, 209.

ZABUSKY, N. J. & KRUSKAL, M. D. 1965 Interaction of solitons in a collisionless plasma and the recurrence of initial states. *Phys. Rev. Lett.* **15**, 240–243.